Origin of water masses in Floridan Aquifer System revealed by ^{81}Kr

REIKA YOKOCHI[1*], JAKE C. ZAPPALA[2], ROLAND PURTSCHERT[3] AND PETER MUELLER[2]

[1]Department of the Geophysical Sciences, The University of Chicago, IL 60637, USA
[2]Physics Division, Argonne National Laboratory, Argonne, IL 60439, USA
[3]Climate and Environmental Physics, Physics Institute and the Oeschger Centre for Climate Change Research, University of Bern, 3012 Bern, Switzerland
[*]Corresponding author: yokochi@uchicago.edu

Abstract

Groundwater in coastal aquifers serves as an essential resource in densely populated areas throughout the world. However, hydrological connection to the ocean leaves it at risk of salinization via changes in climate and hydrological cycles. Therefore, an accurate hydrological characterization of coastal aquifers is of the utmost importance. Although localized salinization of shallow aquifers has commonly been studied, geochemical constraints on the time scale of regional freshwater and seawater in coastal aquifers are limited especially in carbonate aquifers. Such information is not only crucial for water resource management, but also for understanding solute flux over the land-ocean boundary and for interpreting the geochemical signatures that each water mass carries. Toward this goal, we report tracer-based, subsurface residence times of groundwater in the Floridan Aquifer System in southern Florida, which is one of the most productive aquifers on Earth. The first application of ^{81}Kr—an emerging tracer of old groundwater—to this aquifer has identified freshwater recharge during the last glacial period as anticipated from previous studies using other geochemical tools including radiocarbon, stable isotopes and noble gas concentrations. Moreover, freshwater of Holocene age was also detected at 100 km-distance from the recharge area, suggesting the possibility of an active flow system in the upgradient region. A contribution of fossil seawater that predates the last glacial maximum was locally identified, suggesting slow seawater circulation and limited but significant solute flux from the ocean into the aquifer for dolomitization. This also implies that the deep saline coastal groundwater can potentially serve as a paleo-seawater archive.

Keywords: Floridan Aquifer System, radiokrypton isotopes, groundwater dating, fossil seawater, coastal dolomitization

1. Introduction

High population density in coastal regions causes elevated water demand and increased levels of surface water pollution, resulting in severe dependence on and frequent overexploitation of coastal aquifers. Although understanding of the coastal aquifer system in its entirety is ideal for an efficient management of this valuable water resource, most studies only concern shallow portions directly relevant to exploitation. The primary reason for this is their complexity: Coastal aquifers embody geochemical boundaries where saline- and freshwater masses of contrasting chemical compositions meet and cause chemical disequilibrium. In addition to the hydraulic gradient and conductivity, the groundwater flow is driven by the variable density of fluids and by water-rock interactions causing dissolution and/or cementation. Furthermore, sea level fluctuation directly impacts the hydraulic gradient and thus the flow properties of the aquifer. At the same time, these geochemical and hydrological interactions make coastal aquifers potential messengers of the changes in hydrological cycles, the long-term geochemical flux of elements across the land-ocean boundaries, and fossil geochemical signatures.

As a typical example of coastal aquifers, the Floridan Aquifer System (FAS) produces 4.6 billion m^3/year of fresh and brackish water [1]. It serves as a primary source of drinking water to a local population of over 10 million people in Florida, and supports irrigation of over 2 million acres [2]. Additionally, the FAS's upward leakage nurtures thousands of lakes, springs, wetlands and the ecosystems they foster. Having low topographic relief with an altitude mostly below 30 masl, much of the region overlying this aquifer was cyclically inundated during the Pleistocene. The resultant changes in hydraulic head likely altered the rates and pattern of freshwater flow and delineated the landward seawater invasion that increased the salinity of the aquifer [3]. In support of this hypothesis, multi-tracer studies reported concomitant occurrences of colder noble gas recharge temperatures with D- and ^{18}O-enrichments downgradient of the FAS compared to modern recharge in southeastern Georgia [4,5] and in the broad region of south Florida [6]. These observations were interpreted as a result of fossil meteoric water recharged during the last glacial period (LGP), followed by sluggish flow and limited recharge after the sea level rise.

Groundwater age structure of the aquifer would ideally provide information on the timing of recharge, mixing of different water bodies, and spatially- and temporally integrated groundwater flow rates to corroborate or refute the hypothesis. Such data would also allow an assessment of the origin of salinity, which is the primary obstacle of economic water use in the region. The most common dating tracers of groundwater covering Pleistocene timescales are ^{14}C and ^{36}Cl. However, application of ^{14}C is hampered due to water-rock interaction with the carbonate reservoir rocks, making the interpretation complex [7]. The high salinity of these groundwaters also complicates the interpretation of ^{36}Cl data in terms of residence time. Thus, due to the lack of appropriate dating tracers, previous studies primarily relied on indirect time constraints as described above.

Krypton-81 ($t_{½}$= 229±11 kyr) is an emerging tracer in groundwater dating over the timescales of interest here [8]. Its chemical inertness and simple source function make the age interpretation easier and more reliable compared to other tracers such as radiocarbon and ^{36}Cl [9]. A detection of the extremely low modern atmospheric isotopic abundance of ^{81}Kr ($^{81}Kr/Kr = 9.3±0.3 \times 10^{-13}$, [10]) and ^{85}Kr ($t_{½}$= 10.78 yr, $^{85}Kr/Kr \sim 10^{-11}$), which serves as an indicator of young water mixing, requires a dynamic range far beyond conventional noble gas mass spectrometers. Instead, it relies on Atom Trap Trace Analysis (ATTA; [11]), an isotope-selective, laser-based atom counting method. Since the first developments [11] the ATTA method has significantly improved in sensitivity [12, 13]. Along with advances in krypton sample collection and preparation techniques [14-16] it has developed into a practical groundwater dating approach. Application of the tracer in several studies unveiled the time scale of water flow in continental aquifers [17,18]. Furthermore, ^{81}Kr served as an additional constraint to resolve mixing of waters of different age and origin [19,20]. First applications of radiokrypton isotopes in a coastal aquifer along the Mediterranean demonstrated the usefulness of noble gas radioisotopes in revealing the presence of hydraulic connections between the ocean and the aquifer that had long been thought isolated [21]. In this study, we report noble gas radionuclide and radiocarbon isotopic abundances of groundwater in the southern portions of the Florida peninsula. While the data confirmed a major freshwater recharge during the LGP as inferred from other geochemical tracers, they also revealed an active freshwater recharge in the upgradient of the aquifer

during the Holocene and the preservation of fossil seawater that encroached prior to the last glacial maximum (LGM).

2. Hydrologeological background

The Floridan aquifer system (FAS) underlies the entire state of Florida and beyond, consisting of a sequence of hydraulically connected carbonate rocks of Paleocene to Miocene age [22]. The Upper Floridan Aquifer (UFA) contains the highly permeable Suwanee Limestone (Oligocene), Ocala Limestone (upper Eocene) and upper portion of the Avon Park Formation (middle Eocene). The Avon Park Formation includes a sub-regionally extensive high permeability zone (Avon Park Permeable Zone, APPZ; [23]) and the low permeability middle Avon Park composite unit (MCU), which separates the UFA and the Lower Floridan Aquifer (LFA) with dense gypsiferous limestone and chalky limestone. The LFA consists of the lower Avon Park Formation, Oldsmar Formation and upper permeable parts of the Cedar Keys Formation, of upper Paleocene to lower Eocene age. The water quality of the LFA is brackish to saline in south Florida where these carbonates extend up to 100 km to the east beneath the Atlantic and about 200 km into the Gulf of Mexico.

The FAS is confined by more than 30 m of the Hawthorn Formation in the study area. In central and southern Florida, the recharge to the UFA occurs near the potentiometric mound at Polk City, and the flow is south and outward (east and west) from the central ridge of the peninsula according to the predevelopment potentiometric surface (Fig.1a; [24]). Hydrological models of the predevelopment system suggested that a majority (88%) of recharged groundwater flows rapidly in the unconfined zone and discharges to the surface (springs, lakes and streams). In confined parts of the aquifer, the remaining small fraction flows sluggishly and discharges by diffuse upward leakage [24].

The origin of chloride in this aquifer system has always been attributed to seawater. Under debate is the process and timing of the saltwater emplacement: Seawater could have been trapped during deposition or burial of the formation in the Miocene, and the connate seawater may have remained unflushed. It could have encroached laterally from submarine outcrops. An upward movement of the freshwater-saltwater

boundary could have immersed the aquifer in saltwater. Saline water could also have leaked upward above the freshwater-saltwater boundary through structural discontinuities such as faults, fractures, and sinkholes [25]. Finally, geothermal heating and dispersive mixing of saline and freshwater may have driven a convective upwelling of *young* seawater from high permeability zones in southern Florida [26]. This circulation could serve as a major solute supply for diagenetic reactions including dolomitization [27,28]. In the study area of south Florida, groundwater movement in the LFA is landward along the Straits of Florida where the Floridan aquifer system outcrops below sea level at the edge of the plateau. The highly permeable cavernous and fractured dolomite of the LFA is known as the Boulder Zone, hosting saline water chemically comparable to seawater [26]. The saline water in the Boulder Zone is characterized by elevated ^{14}C activity (37-63 pMC; [3]), interpreted as a young seawater contribution.

3. Sampling sites and methods

In order to address the presence of LGP freshwater and Holocene seawater in the FAS, samples were collected at three sites (Fig. 1a), each of which had two or three wells at different depths (Fig. 1b). Site and well IDs used here conform with the database of the South Florida Water Management District, and are common with Morrissey et al. [6]. The first site (OKF105) is in the region where probably the youngest LGP freshwater resides according to ^{4}He concentrations, as reported by Morrissey et al. [6]. Two other sites downgradient (LAB and I75) have high salinity at depth. Five shallower wells tap upper permeable zones of the UFA (OKF105-U, LAB-MZ1, LAB-MZ2, I75-MZ1 and I75-MZ2), whereas two have screens open to APPZ (OKF105-M, LAB-PW2: [23]). The deepest well at the I75 site (I75-MZ3) taps the uppermost permeable zone of the LFA, bearing fluid with seawater-like chemical composition. The OKF105-U well taps a hydrologically comparable zone to OKF42 reported in Morrissey et al. [6] and the 'Lock S65C well (flow path ID 3.4)' reported in Plummer and Sprinkle [7]. A radiocarbon-based residence time of OKF42 was estimated to be 27.3 kyr after thorough adjustment for water-rock interaction [7]. Morrissey et al. [6] characterized groundwater from four of the freshwater wells (OKF42, LAB-MZ1, LAB-MZ2 and I75-MZ2) as glacial recharge based on the relatively low noble gas recharge temperature ranging

19.3-21.0 °C. The saline water sample, I75-MZ3, was categorized as 'Holocene saltwater'.

Our sampling campaign took place in June 2015 in southern Florida. In the field, temperature, pH and conductivities were measured and water samples were collected for analyses of major ion chemistry. These in-situ and chemical data are available from the DBHYDRO database of the South Florida Water Management District [29]. Bulk gas samples were collected from groundwater using a field degassing device based on a commercial membrane contactor (Liqui-Cel Extra-Flow: [14]). A few hundred liters of groundwater were processed at each well to acquire sufficient quantity of Kr. Dissolved gas extracted from groundwater was compressed into gas cylinders, typically at 2-4 bars, and shipped to the University of Chicago for Kr extraction [14, 30]. The abundances of radiokrypton isotopes were measured via ATTA at Argonne National Laboratory [12]. During the Kr purification, gas splits of ~50 ml STP were set aside for the analyses of ^{14}C in CO_2 [31]. Cryogenically separated CO_2 was sealed off in 6-mm Pyrex tubes and sent to the University of Georgia Accelerator Mass Spectrometry (AMS) facility where CO_2 was graphitized with Fe catalyst for ^{14}C analysis. A fraction of the bulk gas (~15L) was sent to the University of Bern for the analyses of ^{39}Ar activity, following Ar purification [15].

4. Results

In all samples, ^{85}Kr was below 1% of modern atmospheric activity, indicating that there was no significant downward leakage of shallow (younger, <50 years) groundwater or atmospheric contamination during sampling and Kr purification (Table 1). Furthermore, this also strictly eliminates the possibility of major contamination from post-1970 drilling fluids. The isotopic abundances of ^{81}Kr were between 89 pMKr (percent Modern Kr) and modern, suggesting relatively young (<40 kyr) apparent groundwater residence times (Table 2). All but one sample had low (<2 pMC) ^{14}C activity. Two measurements of ^{39}Ar were close to the background level (Table 1).

At the OKF105 site, which is closest to the recharge area, the shallower well (OKF105U) had modern ^{81}Kr activity suggesting recharge after Holocene transgression. The longer apparent residence time based on ^{14}C (31 kyr) can be attributed to an addition of ^{14}C-dead C (hereafter "dead C") from the reservoir

carbonate rock as discussed below. Four deeper (OKF105M) or downgradient (LAB-MZ1, LAB-MZ2 and I75-MZ1) samples with low seawater contribution (i.e. low salinity) show ^{81}Kr activities that agree with the postulated glacial recharge for the fresh groundwater of the UFA in southern Florida [6, 7], ranging from 17±10 to 39±11 kyr. The deep sample from the first permeable zone of the Lower Floridan Aquifer (I75-MZ3) showed discordant apparent ages of 13.7 kyr for ^{14}C and 35±11 kyr for ^{81}Kr, suggesting a mixing of multiple water bodies with different ages. The chemical composition of this sample is comparable to modern seawater. Using both age-constraints suggests that I75-MZ3 contains seawater from different time periods; one young enough to contribute a ^{14}C activity of 18.1 pMC but background level ^{39}Ar and ^{85}Kr activities, and the other old enough to cause more than 10 pMKr depletion in ^{81}Kr. Below we analyze the age structure and the time scale of the seawater movement in this coastal aquifer.

5. Discussions

5.1 The rate of C exchange

As reviewed by Plummer and Glynn [32], the first generation of attempts to correct for geochemical dilution of the ^{14}C signals focused on the processes occurring in the recharge zone under open-system conditions, where ^{14}C-depleted soil carbonates and other minerals were dissolved. Subsequently, a geochemical inverse modeling code, NETPATH [33], additionally tracked time-integrated aqueous reactions in the aquifer to deduce 'adjusted' ^{14}C abundances. However, data for defining complete geochemical reaction schemes are not always available. As a simpler alternative, Han et al. [34] introduced a graphical method involving only $\delta^{13}C$ as a model constrain. In the graphical method, they defined a 'zero-age' line that ties the recharge composition (high ^{14}C and low $\delta^{13}C$) and another end-member representing the aqueous reaction product (^{14}C-free and high $\delta^{13}C$ for carbonate). The deviation of ^{14}C from this line is interpreted as a result of aging (Fig 2). In a modified version of the graphical model [35], the reaction is assumed to be a first-order rate process, with the reaction rate proportional to the $\delta^{13}C$ gradients ($\Delta^{13}C$) between evolving DIC and the reactant solid ($\delta^{13}C_E$) as described by Han et al. [35]:

$$\frac{d\delta^{13}C_{DIC}(t)}{dt} = \lambda_{13}\left(\delta^{13}C_E - \delta^{13}C_{DIC}(t)\right) \quad (1)$$

$$\frac{d^{14}C_{DIC}(t)}{dt} = -(\lambda_{14} + \lambda_{13})^{14}C_{DIC}(t) \quad (2)$$

where λ_{14} and λ_{13} are the radioactive decay constant of ^{14}C and the reaction rate constant of DIC, respectively. The sum $\lambda_{13} + \lambda_{14}$ represents the apparent ^{14}C decay constant that, if known, can be used for the calculation of "corrected" ^{14}C ages. The co-evolution of radiocarbon activity and δ^{13}C composition is described by:

$$\frac{Ln\left[\frac{^{14}C_{DIC}}{^{14}C_0}\right]}{\lambda_{14}+\lambda_{13}} = \frac{Ln\frac{\left[\delta^{13}C_E-\delta^{13}C_{DIC}\right]}{\left[\delta^{13}C_E-\delta^{13}C_0\right]}}{\lambda_{13}} \quad (3)$$

Using a thorough geochemical study of the UFA, Plummer and Sprinkle [7] determined the necessary parameters for the graphical approach to be $^{14}C_0$ = 33.23 pMC, $\delta^{13}C_0 = -11.1$ ‰, and $\delta^{13}C_E = +1.15$ ‰. Fig. 2 plots the δ^{13}C -^{14}C data as well as the δ^{13}C composition against apparent ^{81}Kr ages, together with the modeled evolution curves for λ_{13}= λ_{14}, λ_{14}/2, and λ_{14}/4. Among the five samples with limited seawater contribution, the respective λ_{13} varies between λ_{14} and λ_{14}/4, corroborating the difficulty of accurately determining the groundwater subsurface residence time in carbonate aquifers using ^{14}C. However, the resulting apparent ^{14}C half-life in the aquifer ranges between 2860-4580 years, significantly lower than the radioactive decay half-life. The monitoring well closest to the recharge zone (OKF105-U) taps the aquifer equivalent of sample 3.4 reported in [7]; the geochemical mass balance approach and the graphical approach both led to an adjusted ^{14}C age of >20kyr, whereas ^{81}Kr indicates a much shorter subsurface mean residence time. The upper ^{81}Kr age limit of the OKF105U sample with low ^{14}C abundance of 2.3 pMC indicates rapid water-rock interaction resulting in a ^{14}C decline, corresponding to a λ_{13} value of >0.00042 yr^{-1} or an apparent half-life of < 1650 years. A rapid deterioration of the radiocarbon signal in another carbonate aquifer had recently been reported using ^{39}Ar, where a comparable apparent half-life of ~3700 years was estimated [36].

5.2 Multicomponent mixing

The high salinity of two samples, I75-MZ2 and LAB-PW2, suggests contribution of seawater. The fractions of seawater components were estimated by NETPATH [33], using chloride contents of fresh groundwater in the recharge area (Polk City, Well 1.1 in [7]) and modern seawater. Among collected samples, the seawater contribution increases with depth and proximity to the coast, and ranges from a few percent near the recharge area to unity at I75-MZ3 in the Boulder Zone (Table 1). The fractional contribution of seawater in I75-MZ2 and LAB-PW2 are 19% and 47%, respectively. The discordant ^{14}C and ^{81}Kr ages of I75-MZ3 clearly indicate the contribution of seawater bodies with different residence times as mentioned above. At I75-MZ3, measured chloride contents found in the DBHYDRO database for the 2004 to 2016 time period varied between 18,070 and 21,000 mg/L. This variation could be attributed to a changing contribution of trace fresh groundwater as well as analytical inaccuracy. The proportion of glacial seawater in comparison to recent seawater could also be a factor since the former was more saline than the latter by 2.7 to 6.9 % [37]. Given the uncertainty, we will set limits on residence times of two water masses without presuming the paleo-seawater contribution.

An observed activity concentration normalized to modern atmospheric activity, $^{i}R_{ob}$, of a radioactive isotope *i*, with a decay constant λ_i, of two component mixture is given by the mixing fraction *f* and the residence time of components 1 and 2 (t_1 and t_2) as:

$$^{i}R_{ob} = f \cdot \ ^{i}R_{1x} \cdot e^{-\lambda_i t_1} + (1-f) \cdot \ ^{i}R_{2x} \cdot e^{-\lambda_i t_2} \qquad (4)$$

$^{i}R_{1x}$ and $^{i}R_{2x}$ are the initial isotopic abundances normalized to modern atmospheric activity in each component. The concentrations of DIC, Kr and Ar are assumed to be comparable for the two components in the following discussion. The equations for a general case with variable concentrations are listed in Supplementary Information (*S.I.*) 1, and the effect is briefly discussed at the end of this section.

For a given *f* , determined from chloride contents using NETPATH for LAB-PW2 and I75-MZ2, a measured radionuclide abundance defines a curve representing the relation between t_1 (freshwater) and t_2 (seawater). The observed radiocarbon abundances are considered here as lower limits because they have

been affected by various amounts of carbonate-derived dead carbon as shown above. This implies that deduced ages are considered upper limits, and that the actual ages could be younger. Plotting the ^{81}Kr and ^{14}C constraints together for each data set (Fig 3a,b), the range of mean residence times of each component can be depicted as the segment of the ^{81}Kr curve falling within the range defined by ^{14}C activity (shown as shaded area in Fig 3a,b). The probability density functions (pdf) of ages were numerically deduced using Eq.4 for ^{81}Kr and ^{14}C via Monte Carlo simulation. In the process, the ^{81}Kr abundances were assumed to have a Gaussian distribution whereas all possible ranges of ^{14}C activities (i.e. from measured values to unity with uniform distribution) were investigated. As an additional constraint, it is assumed that the residence time of the water mass is older than the lower bound of the water mass upgradient. Only the sets of ages which satisfy hydrological constraints were accepted, and the simulation continued until 10,000 sets of parameters were obtained. The results are listed in Table 2 and plotted in Fig.4. Due to the truncated distribution of the deduced ages in some cases and the steep ^{14}C curves compared to ^{81}Kr, the pdfs of the ages do not always have normal distribution. For this reason, we report medians and median absolute deviations of each parameter in Table 2 for mixed water masses. The details of the calculation are described in *S.I.*2.

The ^{81}Kr age constraint falls within that of ^{14}C for the mid-depth coastal sample (I75-MZ2) so that the possible age range is simply bound by the hydrological age limits along the ^{81}Kr curve: t_1=16±4.9 kyr (freshwater) and t_2=28±21 kyr (seawater). Further inland, for the groundwater collected from the formation with relatively high transmissivity (LAB-PW2 from APPZ), the two intercepts of the ^{81}Kr-^{14}C curves provide two different ranges of scenarios (Fig 3b). As an additional constraint, this well is hydrologically downgradient of freshwater at the OKF105M site and saline water at the I75-MZ3 site tapping 200 m shallower and 50 km further inland. Therefore, it appears more realistic that the seawater is the older component (see the data analysis of I75-MZ3 below), resulting in t_1= 10±2.5 kyr (freshwater) and t_2 =68±15 kyr (seawater). In both cases, freshwater recharge occurred between the early Holocene and late LGP.

As the contributing fraction *f* of each component could not be determined for I75-MZ3, the possible ranges of residence times for the two seawater bodies are estimated based solely on radionuclides. When

one considers discordant apparent ages of ^{14}C and ^{81}Kr with significantly different decay constants ($\lambda_{14} >> \lambda_{81}$) the residence time of the younger component (1) can be approximated by assuming that the contribution of ^{14}C from the older reservoir (2) is negligible [$\exp(-\lambda_{14} t_2)\ (1-f) \sim 0$]:

$$t_1(f) \sim \ln\left[\frac{^{14}R}{f}\right]^{-1/\lambda_{14}} \quad (5)$$

Therefore, provided another tracer with relatively short half life, e.g. ^{39}Ar, the intersection of the two curves will define the residence time of the younger water mass t_1. For I75-MZ3, the curves defined by ^{39}Ar and ^{14}C data are shown in Fig. 3c. Because the ^{39}Ar data represents an upper abundance limit, its curve defines the lower age limit. Measured radiocarbon abundances are again considered as a lower limit as discussed leading to a ^{14}C curve that defines the upper age limit. The area bound by the two curves in Fig. 3c represents the possible combinations of parameters. The intercept gives the lower limit for f and t_1 of 0.185 and 167 years, respectively.

For a small $\lambda_{81} t_1$ (< 0.1, i.e. limited decay of ^{81}Kr in the reservoir 1 or t_1 <33 kyr for ^{81}Kr), an approximation $[1-\exp(-\lambda_{81} t_1)]/\ \lambda_{81} \sim t_1$ leads to:

$$t_2(f) \sim \ln\left[\frac{^{81}R - f\left\{1+\frac{\lambda_{81}}{\lambda_{14}}\ln\left[\frac{^{14}R}{f}\right]\right\}}{1-f}\right]^{-1/\lambda_{81}} \quad (6)$$

Using f as a parametric variable,

$$t_2(t_1) = \frac{\ln\left[^{81}R + \frac{^{14}R(^{81}R + t_1\lambda_{81} - 1)}{e^{-t_1\lambda_{14}} - ^{14}R}\right]}{-\lambda_{81}} \quad (7)$$

The pdf of water mass ages contributing to the I75-MZ3 well were numerically deduced using Eq.5 for ^{39}Ar and ^{14}C and Eq.7 for ^{81}Kr via Monte Carlo simulation assuming uniform distributions for $0 < ^{39}Ar < 0.12$ and $0.181 < ^{14}C < 1$ (see Supplementary Information 2 for details). Obtained ages were $t_1 = 0.84 \pm 0.21$ kyr and $t_2 = 80 \pm 34$ kyr. This water mass is less prone to carbon exchange with carbonates compared to other samples which were freshwater or freshwater-seawater mixtures. When the measured ^{14}C ($^{14}R = 0.181$, $\delta_{14R} = 0.001$

with Gaussian distribution) were used for the calculation, obtained ages were lower, t_1=0.44±0.19 kyr and t_2=44±9.2 kyr. The actual age ranges are probably between the two ranges.

Although it does not direcly add to the specific case presented herein, the upper limit of f can be constrained using only two tracers by the numerator of Eq.6, which needs to be positive. The solution for *f* is expressed with Lambert's *W* function as:

$$f_{max} = -\left[\frac{1}{{}^{81}R\frac{\lambda_{14}}{\lambda_{81}}} \cdot W\left(-\frac{\frac{{}^{81}R}{\lambda_{81}}}{\frac{{}^{14}R}{\lambda_{14}}} e^{-\frac{\lambda_{14}}{\lambda_{81}}}\right)\right]^{-1} \quad (8)$$

Provided comparable C_{DIC}/C_{Kr} in the two seawater masses, one obtains f_{max} = 0.939 and $t_{1,max}$ = 13.6 kyr for I75-MZ3, which does not contradict the ages deduced above. Due to the variability in global climate and seawater chemistry, the concentrations of DIC and Kr could also vary over time. The curve in Fig.3d shifts depending on the relative enrichment of DIC compared to Kr in the older water mass (see *S.I.*1); variations of ± 20 % in this parameter would not significantly affect our conclusion as shown in Fig. 3d. An example on the effect of dead C contribution is also shown in Fig.3d. Higher ^{14}C activity will require a larger contribution of younger water with a corresponding smaller fraction of older water.

5.3 Hydrological and geochemical implications

Previous studies suggested major freshwater recharge of the UFA during sea level low-stand, and a deceleration (thus limited recharge) of groundwater flow accompanying sea level rise that caused a reduction of hydraulic head gradients [3]. Geochemical tracers also suggested that recharge occurred at lower surface temperatures [4-6]. Most ^{81}Kr data of freshwater components from downgradient agree well with this scenario: recharge predominantly during the LGP (< 50 kyr; Fig. 4), and rapid flow (> 5 m/yr) reaching the farthest site, I75, at 240 km distance from the recharge area. A single sample from a shallow well in the upgradient region (OKF105U) showed relatively short residence time (< 6.4 kyr), suggesting an active hydrological cycle in the upgradient region of the UFA where the confining Hawthorn formation is thin (i.e. faster upward leakage). Replicates and further analyses of samples from the upgradient region are highly recommended to confirm this result as it is crucial information for freshwater resource assessment.

It is also noteworthy that samples from two mid-depth wells with lower transmissivities revealed younger ages than the shallower wells with probabilities of 79 % and 76 % for LAB-MZ2 and I75-MZ2 wells, respectively. Provided that the primary discharge of the aquifer system is by upward leakage [24], the longer residence time of the shallower groundwater sampled at wells LAB-MZ1 and I75-MZ1 may result from the aging of water during slow, upward cross-formational flow to shallower depths.

Among the three wells in which a substantial seawater contribution was identified, the deepest coastal well (I75-MZ3) tapping the LFA showed the highest radiocarbon activity. This is in accordance with previous studies, suggesting the presence of relatively young coastal seawater in the aquifer [3,38]. The ^{81}Kr data revealed the presence of an additional older seawater body predating the LGM. A seawater mass of comparable antiquity was also found in the deepest part of the UFA approximately 30 km from the coast (LAB-PW2). According to the hydrological model on the response of the FAS to sea level rise [39], the exchange of seawater and groundwater in south Florida occurs from underlying units and requires a saline water flux from beneath through the MCU. Therefore, the fossil seawater that contributed to the LAB-PW2 well probably percolated up from the LFA. The presence of fossil seawater in the FAS suggests that the timescale of the seawater circulation (Kohout convection) has not been sufficiently rapid to displace the water mass with Holocene seawater. Similarly, Archer [40] reported a hydrological model showing a persistent salinity over a 100-kyr time scale at the Siberian continental margin. More data on the residence time of saline coastal aquifer are necessary to examine the ubiquity of slow water circulation in deep coastal aquifers. The Boulder Zone has been used as a receptacle for oil-field brine and municipal wastewater [3, 41] and this slow circulation implies the stability (i.e. slow dispersion) of injected fluids.

Seawater circulating in coastal aquifers could serve as a major source of solutes for diagenetic reactions, notably dolomitization [27,28]. Carbonate-water interaction rates (or weathering) are of interest because they play a significant role in the global carbon cycle [42]. More specifically, Tipper et al. [43] highlighted dolomite as a significant sink of Mg based on the isotopic mass balance of Mg among geochemical reservoirs. The mean residence time of seawater acquired using ^{81}Kr enables an estimation of the solute flux in the FAS, which is the probable limiting factor of dolomitization. The Boulder Zone

beneath the Florida peninsula extends over 37,000 km^2. With a typical thickness of 0.1-0.2 km and porosity of 0.3, at least 1000 km^3 of seawater is stored within this volume. The long-term flux of seawater through the Boulder Zone could be estimated at about 0.01-0.02 km^3/yr based on the mean residence time of 68 ± 15 kyr at LAB-PW2. Using a reference seawater concentration of 0.566 mol/kg, 0.0547mol/kg and 0.0107 mol/kg, for Cl, Mg and Ca, respectively [44], estimated elemental fluxes in the FAS via Kohout convection would be 9.5, 0.92 and 0.18 × 10^9 mol/year. This Mg flux constitutes 0.02 % of global riverine Mg flux, and 0.9 % of Mg sink by continental carbonate [45].

In an attempt to extrapolate the Mg flux to a global scale, the distribution of coastal karstic aquifers appears to be the best available information [46]; according to their geographic analyses, 151,400 km of global coastlines are characterized by carbonate rocks. The Boulder Zone has a coastline length of 1,300 km, constituting 0.86 % of the global carbonate coastline [47]. Therefore, coastal karstic aquifers could be significant Mg sinks via dolomitization if (i) the Mg flux is similar for every karstic aquifer along coastlines, (ii) the length of the coastlines at surface and in greater depth are comparable, and (iii) the total Mg influx from the ocean is used for dolomitization in the aquifer. While this is certainly an oversimplification, the system may not be limited by Mg flux, thus deserve more detailed studies for quantifying the rate of dolomitization in coastal karstic aquifers compared to the well-documented deposition of Mg-bearing minerals during diagenetic process in deep-sea sediments (e.g. [48]).

The detection of fossil seawater in a coastal aquifer also raises another interesting issue. Paleo-seawater composition during the LGM was estimated mostly based on pelagic sediment pore fluids of drilled cores [37]. These archives were modified from the original compositions by in-situ diffusion, which necessitate model-dependent correction for this secondary effect. As a possible alternative paleo-seawater archive, pore-fluids of drill cores from high-porosity carbonate in the Maldives were reported to have been minimally affected by diffusion [49]. Our study suggests that paleo-seawater of different ages can be stored in coastal aquifer systems. Although water-rock interaction and complex hydrology (e.g. potential of freshwater mixing) could complicate the reconstruction of paleo-seawater composition, an obvious advantage of these water masses compared to the drilled cores is the ease of sample access via existing

wells and the availability of large sample masses, that is also a prerequisite for the analyses of ^{81}Kr to provide a time axis for the encountered seawater masses.

6. Conclusion

The first application of noble gas radionuclide analysis in water samples from the Floridan Aquifer System identified freshwater recharged during the LGP, confirming previous studies based on other geochemical tracers. The new data, which were interpreted in a novel comprehensive multi-tracer framework, also suggest a possibility of fresh groundwater recharge during the Holocene in the upgradient of the aquifer where the confining unit is thinner. Unlike simple aquifer systems where groundwater age progressively increases with the depth and distance from the recharge area, we observed an inverted chronology with older waters at shallower depth at two locations. This can be attributed to slow upward leakage of deep circulating water.

Coastal saline groundwater in the Lower Floridan Aquifer had long been attributed to seawater encroachment during the Holocene marine transgression based on significant radiocarbon activities. The single sample studied here that is tapping the Lower Floridan Aquifer confirmed a relatively young apparent age based on ^{14}C, but also revealed the presence of older seawater predating the LGM via ^{81}Kr. The presence of fossil seawater implies relatively slow circulation and limited solute flux, but the aquifer system may undergo considerable dolomitization over geological time scales. The ability to date the subsurface seawater by ^{81}Kr also makes the FAS a potential archive of paleo-seawater composition. Further studies using ^{81}Kr with an extended set of sampling sites and improved precision is desirable for refining the freshwater flow regime and for examining the potential of the stored saline water as paleo-seawater archives. Near-term developments in ^{81}Kr-dating via the ATTA technique are expected to allow for age determinations of LGP waters with errors below 4 kyr—over a factor of two improvement from what was demonstrated in this study.

Acknowledgements

This work was supported by the Ben Gurion University–Argonne National Laboratory–University of Chicago Collaborative Water Research Initiative. J. C. Z. and P. M. are supported by U.S. Department of Energy, Office of Nuclear Physics, under Contract NoDE-AC02-06CH11357. We thank Emily Richardson, Steven Krupa and Brian Collins from South Florida Water Management District for letting us join their field campaign, sharing their profound knowledge on this aquifer, and for providing input to the draft of the manuscript. Ryan Bernier and Le-Yi Tu are acknowledged for help during groundwater sampling. R.Y. thanks N.C. Sturchio, C. Blättler, D. R. MacAyeal and D. Archer for scientific discussions and advice. R.Y. is grateful to B. Lynch, J. Eason, and PSD Desktop Support for their support.

References

1. Geddes, E., Coonts, S., Collins, B., 2018. Geochemistry of the Upper Floridan Aquifer and Avon Park Permeable Zone Within the South Florida Water Management District. *Technical Publication (Resource Evaluation Section, Water Supply Bureau South, South Florida Water Management District)* WS-47, 1-32. https://www.sfwmd.gov/document/ws-47-geochemistry-upper-floridan-aquifer-and-avon-park-permeable-zone-within-south
2. Bellino, J.C., Kuniansky, E.L., O'Reilly, A.M., Dixon, J.F., 2018. Water Availability and Use Science Program Hydrogeologic Setting, Conceptual Groundwater Flow System, and Hydrologic Conditions 1995 – 2010 in Florida and Parts of Georgia, Alabama, and South Carolina Scientific Investigations Report 2018 – 5030, 115.
3. Meyer, F.W., 1989. Hydrogeology, ground-water movement, and subsurface storage in the Floridan aquifer system in southern Florida. US Geological Survey Professional Paper 1403-G, 64. https://doi.org/10.3133/pp1403G
4. Plummer, L.N., 1993. Stable isotope enrichment in paleowaters of the southeast Atlantic coastal plain, United States. Science 262, 2016–2020. https://doi.org/10.1126/science.262.5142.2016
5. Clark, J.F., Stute, M., Schlosser, P., Drenkard, S., Bonani, G., 1997. A tracer study of the Floridan aquifer in southeastern Georgia: Implications for groundwater flow and paleoclimate. Water Resources Research 33, 281–289.
6. Morrissey, S.K., Clark, J.F., Bennett, M., Richardson, E., Stute, M., 2010. Groundwater reorganization in the Floridan aquifer following Holocene sea-level rise. Nature Geoscience 3, 683–687. https://doi.org/10.1038/ngeo956
7. Plummer, L.N., Sprinkle, C.L., 2001. Radiocarbon dating of dissolved inorganic carbon in groundwater from confined parts of the Upper Floridan aquifer, Florida, USA. Hydrogeology Journal 9, 127–150. https://doi.org/10.1007/s100400000121
8. Lu, Z.T., Schlosser, P., Smethie, W.M., Sturchio, N.C., Fischer, T.P., Kennedy, B.M., Purtschert, R., Severinghaus, J.P., Solomon, D.K., Tanhua, T., Yokochi, R., 2014. Tracer applications of noble gas radionuclides in the geosciences. Earth-Science Reviews 138, 196–214. https://doi.org/10.1016/j.earscirev.2013.09.002
9. Purtschert, R., Yokochi, R., Sturchio, N.C., 2013. Kr-81 dating of old groundwater., in: Suckow, A., Aggarwal, P.K., Araguas-Araguas, L. (Eds.), Isotope Methods for Dating Old Groundwater. International Atomic Energy Agency, Vienna, pp. 91–124.
10. Zappala, J.C., Baggenstos, D., Gerber, C., Jiang, W., Kennedy, B.M., Lu, Z.T., Masarik, J., Mueller, P., Purtschert, R., Visser, A., 2020. Atmospheric ^{81}Kr as an Integrator of Cosmic-Ray Flux on the Hundred-Thousand-Year Time Scale. Geophysical Research Letters 47, 1–7. https://doi.org/10.1029/2019GL086381
11. Chen, C.Y., Li, Y.M.M., Bailey, K., O'Connor, T.P.P., Young, L., Lu, Z.-T., 1999. Ultrasensitive Isotope Trace Analyses with a Magneto-Optical Trap. Science 286, 1139–1141. https://doi.org/10.1126/science.286.5442.1139
12. Jiang, W., Bailey, K., Lu, Z.-T., Mueller, P., O'Connor, T.P., Cheng, C.-F., Hu, S.-M., Purtschert, R., Sturchio, N.C., Sun, Y.R., Williams, W.D., Yang, G.-M., 2012. ATTA-3: An atom counter for measuring ^{81}Kr and ^{85}Kr in environmental samples. Geochimica et Cosmochimica Acta 91, 1–6.

13. Zhang, Z.Y., Ritterbusch, F., Hu, W.K., Dong, X.Z., Gao, C.Y., Jiang, W., Liu, S.Y., Lu, Z.T., Wang, J.S., Yang, G.M., 2020. Enhancement of the ^{81}Kr and ^{85}Kr count rates by optical pumping. Physical Review A 101, 1–10. https://doi.org/10.1103/PhysRevA.101.053429
14. Yokochi, R., 2016. Recent developments on field gas extraction and sample preparation methods for radiokrypton dating of groundwater. Journal of Hydrology 540, 368–378.
15. Riedmann, R.A., Purtschert, R., 2016. Separation of argon from environmental samples for Ar-37 and Ar-39 analyses. Separation and Purification Technology 170, 217–223. https://doi.org/10.1016/j.seppur.2016.06.017
16. Dong, X.Z., Ritterbusch, F., Chu, Y.Q., Gu, J.Q., Hu, S.M., Jiang, W., Lu, Z.T., Yang, G.M., Zhao, L., 2019. Dual Separation of Krypton and Argon from Environmental Samples for Radioisotope Dating. Analytical Chemistry 91, 13576–13581. https://doi.org/10.1021/acs.analchem.9b02716
17. Sturchio, N.C.C., Du, X., Purtschert, R., Lehmann, B.E., Sultan, M., Patterson, L.J., Lu, Z.-T., Muller, P., Bogler, T., Bailey, K., O'Connor, T.P.P., Young, L., Lorenzo, R., Becker, R., El Alfy, Z., El Kaliouby, B., Dawood, Y., Abdallah, A.M.A.A.M.A., Bigler, T., Bailey, K., O'Connor, T.P.P., Young, L., Lorenzo, R., Becker, R., El Alfy, Z., El Kaliouby, B., Dawood, Y., Abdallah, A.M.A.A.M.A., 2004. One million year old groundwater in the Sahara revealed by krypton-81 and chlorine-36. Geophysical Research Letters 31, 2–5. https://doi.org/10.1029/2003GL019234
18. Matsumoto, T., Zouari, K., Trabelsi, R., Hillegonds, D., Jiang, W., Lu, Z.T., Mueller, P., Zappala, J.C., Araguás Araguás, L.J., Romeo, N., Agoun, A., 2020. Krypton-81 dating of the deep Continental Intercalaire aquifer with implications for chlorine-36 dating. Earth and Planetary Science Letters 535, 116120. https://doi.org/10.1016/j.epsl.2020.116120
19. Gerber, C., Vaikmäe, R., Aeschbach, W., Babre, A., Jiang, W., Leuenberger, M., Lu, Z.T., Mokrik, R., Müller, P., Raidla, V., Saks, T., Waber, H.N., Weissbach, T., Zappala, J.C., Purtschert, R., 2017. Using ^{81}Kr and noble gases to characterize and date groundwater and brines in the Baltic Artesian Basin on the one-million-year timescale. Geochimica et Cosmochimica Acta 205, 187–210. https://doi.org/10.1016/j.gca.2017.01.033
20. Yokochi, R., Ram, R., Zappala, J.C., Jiang, W., Adar, E., Bernier, R., Burg, A., Dayan, U., 2019. Radiokrypton unveils dual moisture sources of a deep desert aquifer. Proceedings of the national academy of Sciences 116, 16222–16227. https://doi.org/10.1073/pnas.1904260116
21. Yechieli, Y., Yokochi, R., Zilberbrand, M., Lu, Z., Purtschert, R., Sueltenfuss, J., Jiang, W., Zappala, J., Mueller, P., Bernier, R., Avrahamov, N., Adar, E., Talhami, F., Livshitz, Y., Burg, A., 2019. Recent seawater intrusion into deep aquifer determined by the radioactive noble-gas isotopes ^{81}Kr and ^{39}Ar. Earth and Planetary Science Letters 507, 21–29. https://doi.org/10.1016/j.epsl.2018.11.028
22. Miller, J.A., 1986. Hydrogeologic framework of the Floridan Aquifer System in Florida and in parts of Georgia, Alabama, and South Carolina—Regional Aquifer-system Analysis. U.S. Geological Survey Provessional Paper 1403-B, 91.
23. Reese, R.S., Richardson, E., 2008. Synthesis of the Hydrogeologic Framework of the Floridan Aquifer System and Delineation of a Major Avon Park Permeable Zone in Central and Southern Florida. U.S. Geological Survey Scientific Investigations Report 2007–5207, 66.
24. Bush, P.W., Johnson, R.H., 1988. Ground-water hydraulics, regional flow, and ground-water development of the Floridan aquifer system in Florida and in parts of Georgia, South Carolina. USGS Professional Paper 1403–C, 1–80.

25. Reese, R.S., 2000. Hydrogeology and the Distribution of Salinity in the Floridan Aquifer System, Southwestern Florida. U.S. Geological Survey Water-Resources Investigations Report 98-4253 86.
26. Kohout, F.A., 1965. A hypothesis concerning cyclic flow of salt water related to geothermal heating in Floridan Aquifer. Transactions of the New York Academy of Sciences 28, 249–271.
27. Kaufman, J., 1994. Numerical models of fluid flow in carbonate platforms: implications for dolomitization. Journal of Sedimentary Research A: Sedimentary Petrology & Processes 64 A, 128–139. https://doi.org/10.1306/d4267d2f-2b26-11d7-8648000102c1865d
28. Sanford, W.E., Whitaker, F.F., Smart, P.L., Jones, G., 1998. Numerical analysis of seawater circulation in carbonate platforms: I. Geothermal convection. American Journal of Science 298, 801–828. https://doi.org/10.2475/ajs.298.10.801
29. South Florida Water Management District, 2018. DBHYDRO (Environmental Data) [WWW Document]. URL https://www.sfwmd.gov/science-data/dbhydro
30. Yokochi, R., Heraty, L.J., Sturchio, N.C., 2008. Method for purification of krypton from environmental samples for analysis of radiokrypton isotopes. Analytical Chemistry 80. https://doi.org/10.1021/ac801804x
31. Yokochi, R., Bernier, R., Purtschert, R., Zappala, J., Yechieli, Y., Adar, E., Jiang, W., Lu, Z.-T., Mueller, P., Olack, G., Ram, R., 2018. Field degassing as a new sampling method for 14C analyses in old groundwater. Radiocarbon 60, 349–366.
32. Plummer, N., Glynn, P.D., 2013. Radiocarbon Dating in Groundwater System, in: Suckow, A., Aggarwal, P.K., Araguas-Araguas, L. (Eds.), Isotope Methods for Dating Old Groundwater. International Atomic Energy Agency, Vienna, pp. 33–90.
33. Plummer, L.N., Prestemon, E.C., Parkhurst, D.L., 1994. An interactive code (NETPATH) for modeling NET geochemical reactions along a flow PATH, version 2.0. U.S. Geological Survey Water-Resources Investigations Report 94–4169, 130 p.
34. Han, L.F., Plummer, L.N., Aggarwal, P., 2012. A graphical method to evaluate predominant geochemical processes occurring in groundwater systems for radiocarbon dating. Chemical Geology 318–319, 88–112. https://doi.org/10.1016/j.chemgeo.2012.05.004
35. Han, L.F., Niel Plummer, L., Aggarwal, P., 2014. The curved ^{14}C vs. $\delta^{13}C$ relationship in dissolved inorganic carbon: A useful tool for groundwater age- and geochemical interpretations. Chemical Geology 387, 111–125. https://doi.org/10.1016/j.chemgeo.2014.08.026
36. Avrahamov, N., Yechieli, Y., Purtschert, R., Levy, Y., Sultenfuß, J., Vergnaud, V., Burg, A., 2018. Characterization of a carbonate karstic aquifer flow system using multiple radioactive noble gases (^{3}H- ^{3}He , ^{85}Kr , ^{39}Ar) and C as environmental tracers. Geochimica et Cosmochimica Acta 242, 213–232. https://doi.org/10.1016/j.gca.2018.09.009
37. Adkins, J.F., McIntyre, K., Schrag, D.P., 2002. The salinity, temperature, and δ18O of the glacial deep ocean. Science 298, 1769–1773. https://doi.org/10.1126/science.1076252
38. Sprinkle, C.L., 1989. Geochemistry of the Floridan aquifer system in Florida and in parts of Georgia, South Carolina, and Alabama. US Geological Survey Professional Paper 1403-B, 101. https://doi.org/10.3133/pp1403i
39. Hughes, J.D., Vacher, H.L., Sanford, W.E., 2009. Temporal response of hydraulic head, temperature, and chloride concentrations to sea-level changes, Floridan aquifer system, USA. Hydrogeology Journal 17, 793–815. https://doi.org/10.1007/s10040-008-0412-0
40. Archer, D., 2015. A model of the methane cycle, permafrost, and hydrology of the Siberian continental margin. Biogeosciences 12, 2953–2974. https://doi.org/10.5194/bg-12-2953-2015

41. Maliva, R.G., Guo, W., Missimer, T., 2007. Vertical migration of municipal wastewater in deep injection well systems, South Florida, USA. Hydrogeology Journal 15, 1387–1396. https://doi.org/10.1007/s10040-007-0183-z
42. Gaillardet, J., Calmels, D., Romero-Mujalli, G., Zakharova, E., Hartmann, J., 2019. Global climate control on carbonate weathering intensity. Chemical Geology 527, 118762. https://doi.org/10.1016/j.chemgeo.2018.05.009
43. Tipper, E.T., Galy, A., Gaillardet, J., Bickle, M.J., Elderfield, H., Carder, E.A., 2006. The magnesium isotope budget of the modern ocean: Constraints from riverine magnesium isotope ratios. Earth and Planetary Science Letters 250, 241–253. https://doi.org/10.1016/j.epsl.2006.07.037
44. Millero, F.J., Feistel, R., Wright, D.G., McDougall, T.J., 2008. The composition of Standard Seawater and the definition of the Reference-Composition Salinity Scale. Deep-Sea Research Part I: Oceanographic Research Papers 55, 50–72. https://doi.org/10.1016/j.dsr.2007.10.001
45. Wilkinson, B.H., Algeo, T.J., 1989. Sedimentary carbonate record of calcium-magnesium cycling. American Journal of Science 289, 1158–1194. https://doi.org/10.2475/ajs.289.10.1158
46. Goldscheider, N., Chen, Z., Auler, A.S., Bakalowicz, M., Broda, S., Drew, D., Hartmann, J., Jiang, G., Moosdorf, N., Stevanovic, Z., Veni, G., 2020. Global distribution of carbonate rocks and karst water resources. Hydrogeology Journal 28, 1661–1677. https://doi.org/10.1007/s10040-020-02139-5
47. Williams, L.J., Dixon, J.F., 2015. Digital Surfaces and Thicknesses of Selected Hydrogeologic Units of the Floridan Aquifer System in Florida and Parts of Georgia, Alabama, and South Carolina, U.S. Geological Survey Data Series 926. Virginia.
48. Higgins, J.A., Schrag, D.P., 2010. Constraining magnesium cycling in marine sediments using magnesium isotopes. Geochimica et Cosmochimica Acta 74, 5039–5053. https://doi.org/10.1016/j.gca.2010.05.019
49. Blättler, C.L., Higgins, J.A., Swart, P.K., 2019. Advected glacial seawater preserved in the subsurface of the Maldives carbonate edifice. Geochimica et Cosmochimica Acta 257, 80–95. https://doi.org/10.1016/j.gca.2019.04.030
50. Bollhöfer, A., Schlosser, C., Schmid, S., Konrad, M., Purtschert, R., Krais, R., 2019. Half a century of Krypton-85 activity concentration measured in air over Central Europe: Trends and relevance for dating young groundwater. Journal of Environmental Radioactivity 205–206, 7–16. https://doi.org/https://doi.org/10.1016/j.jenvrad.2019.04.014

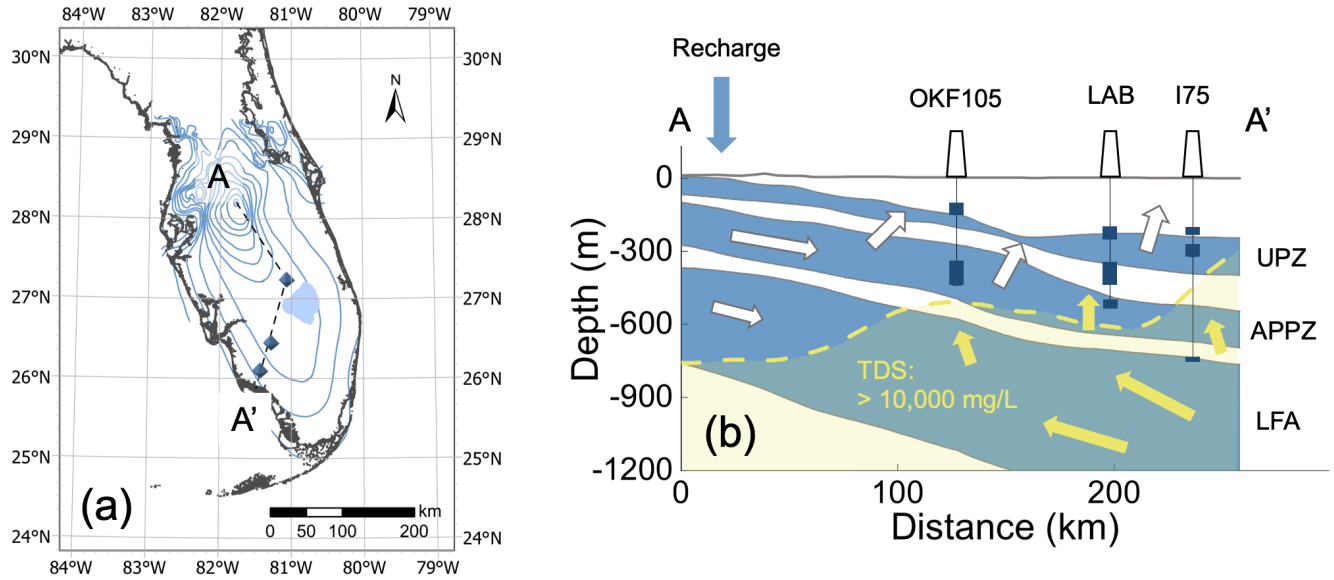

Figure 1: (a) Locations of the three sampling sites (blue diamonds), recharge area (Polk City, 'A' in the map), and the hydraulic gradient of Upper Floridan Aquifer (contour lines from [23]). Each site had 2 or 3 nested wells. (b) Cross section along the dashed line A-A' in (a) generated using the digital data provided by USGS [47]. 'UPZ' and 'APPZ' represent the upper permeable zone and Avon Park Permeable Zone of the Upper Floridan Aquifer, whereas LFA stands for the Lower Floridan Aquifer. The yellow dashed line is the isochemical chloride concentration line at 10,000 mg/L. Yellow and white arrows show anticipated flow of saline water and freshwater. Vertical exaggeration is by a factor of 50.

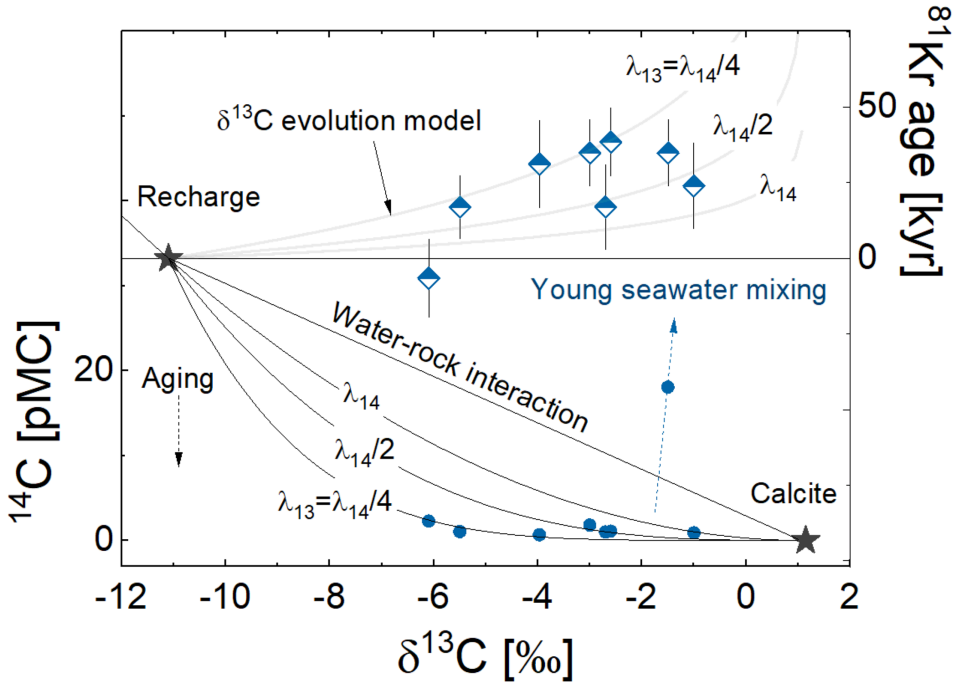

Figure 2: (top) Apparent ^{81}Kr age vs. δ^{13}C data and (bottom) radiocarbon abundances vs. δ^{13}C data, shown with anticipated evolution curves assuming different time constants for the deviation of δ^{13}C (λ_{13}) from the value in the recharge area. The uncertainties on δ^{13}C and ^{14}C are comparable to or less than the size of the symbols.

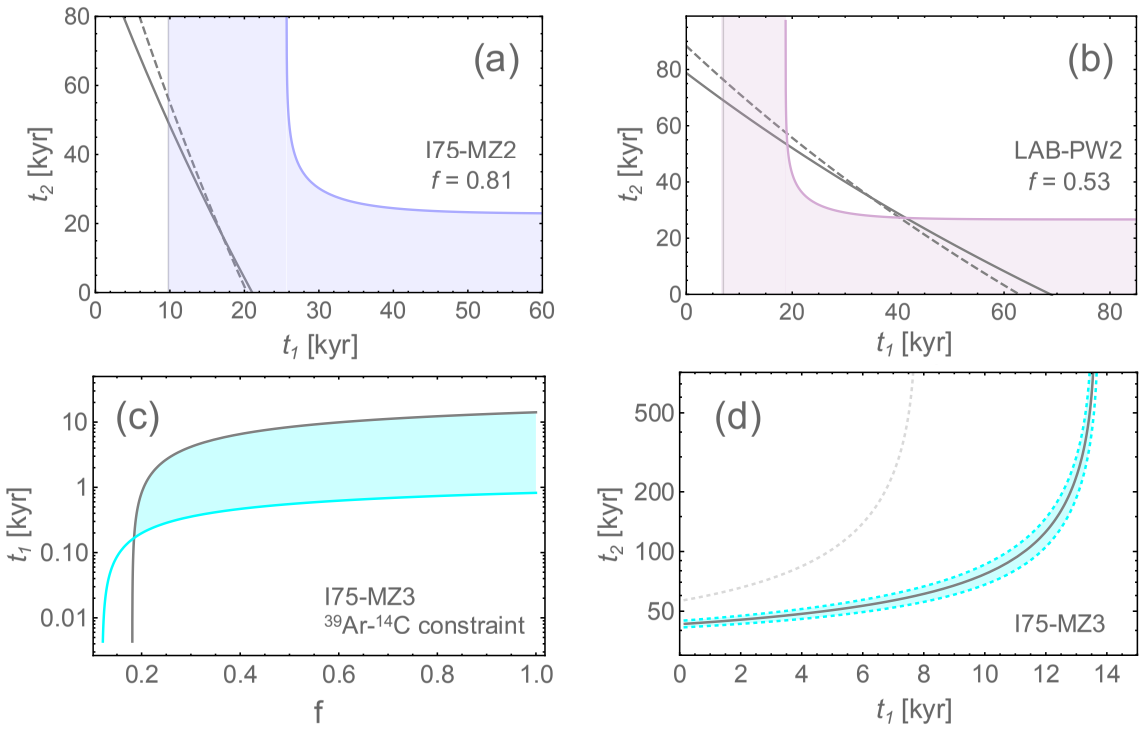

Figure 3: Mean residence times assuming two component mixing. Solid gray lines represent ^{81}Kr constraints and colored lines represent that of ^{14}C. Initial radiocarbon abundances of freshwater is set at 33 pMC following [7]. Dashed gray lines are cases for different enrichment factors of Kr in the younger seawater or freshwater reservoirs (R_E): (a) I75-MZ2 with R_E=1.2, (b) LAB-PW2 with R_E=1.2; (c) The t_1 of I75-MZ3 as a function of f constrained by ^{39}Ar (blue) and ^{14}C (gray). The colored zone is the possible range; (d) Possible t_1 -t_2 combinations constrained by the ^{14}C and ^{81}Kr abundances. Solid gray line assumes comparable DIC/Kr for two seawater bodies, and the blue zone represent DIC-enrichment of +/- 20%. If measured value had been compromised by the addition of dead C, the correction results in longer t_2 (an example shown as gray dotted line for 50% dead C contribution.

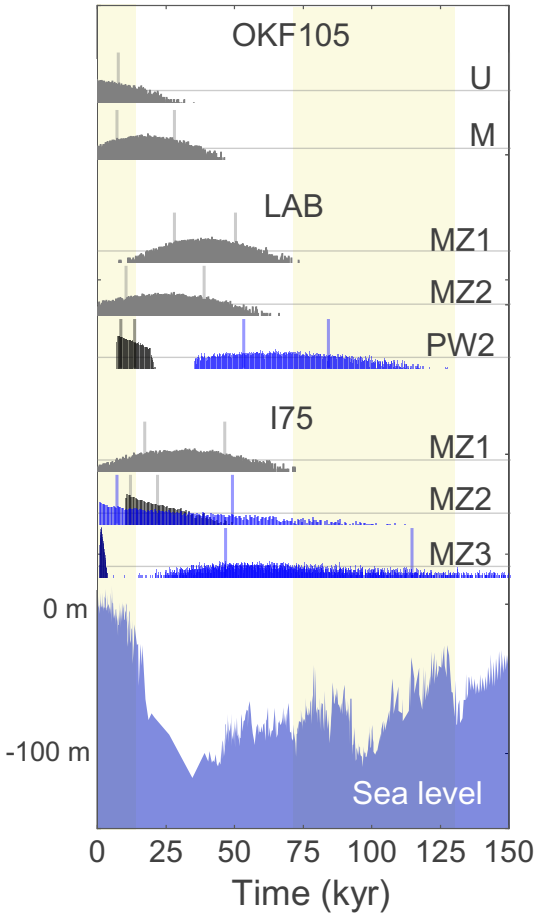

Figure 4: Logarithm of probability density function (pdf) of groundwater ages shown with sea level change over time. The details of the calculation method via Monte Carlo simulation is described in *S.I.*2. Gray histograms represent freshwater, whereas blue ones represent seawater. Gray horizontal lines are 1% probability within the kyr. Vertical lines bound 1σ limits for unmixed water mass and median absolute deviation for mixed water masses.

Table

Table 1: Isotopic abundances of noble gas radionuclides, radiocarbon and stable carbon isotopic compositions, Cl concentration, and the fractional contributions of seawater. Errors are at 1-σ. † Values taken from a well within the recharge area at Polk City from [7]. ‡ 90% confidence level. * Radiokrypton isotopes, ^{14}C and δ^{13}C data were reported in [31]. ** From [50].

	^{85}Kr	^{81}Kr	^{39}Ar	δ^{13}C	^{14}C	Cl	Seawater
	dpm/cc	pMKr	pMAr		pMC	ppm	Fraction
OKF105U*	0.44 ± 0.1	102 ± 4		-6.1	2.3	153	0.02
OKF105M*	0.14 ± 0.09	95 ± 3	17±11	-5.5	1.0	513	0.03
LAB-MZ1	0.2 ± 0.05	89 ± 3		-2.6	1.1	733	0.04
LAB-MZ2	0.27 ± 0.09	93 ± 4		-1	0.9	541	0.03
LAB-PW2 *	0.16 ± 0.1	90 ± 3		-3	1.8	8700	0.47
I75-MZ1	0.75 ± 0.19	91 ± 4		-3.97	0.7	1500	0.07
I75-MZ2	0.2 ± 0.09	95 ± 4		-2.7	1.0	4003	0.19
I75-MZ3 *	<0.34‡	90 ± 3	<12	-1.5	18.1	20165	1
Recharge†				-11.1	33	6.9	0
Seawater						19353	1
Modern air	76**	≡ 100	≡ 100				

Table 2: Groundwater age deduced from ^{81}Kr, ^{39}Ar and ^{14}C isotopic abundances as well as mixing contributions. Apparent ^{81}Kr ages of mixed samples are also listed.

	Water mass 1 kyr	Water mass 2 kyr	Apparent ^{81}Kr age
OKF105U	< 6.4		
OKF105M	17 ± 10		
LAB-MZ1	39 ± 11		
LAB-MZ2	24 ± 14		
LAB-PW2	10 ± 2.5	68 ± 15	35 ± 11
I75-MZ1	31 ± 15		
I75-MZ2	16 ± 4.9	28 ± 21	17 ± 14
I75-MZ3	0.84 ± 0.21	80 ± 34	35 ± 11
Water type	*Freshwater or young seawater*	*Seawater*	

CRediT author statement

Reika Yokochi: Conceptualization, Investigation (Field sample collection, sample processing), Funding acquisition, Writing - Original Draft, **Jake Zappala:** Investigation (Radiokrypton analyses), Methodology, Writing - Review & Editing, **Ryan Bernier:** Investigation (Field sample collection), **Roland Purtschert:** Investigation (39Ar analysis), Resources, Validation, Writing - Review & Editing, **Peter Mueller:** Writing - Investigation (Radiokrypton analyses), Resources, Review & Editing, Funding acquisition

Declaration of interests

☒ The authors declare that they have no known competing financial interests or personal relationships that could have appeared to influence the work reported in this paper.

☐The authors declare the following financial interests/personal relationships which may be considered as potential competing interests:
